Macromolecules

pubs.acs.org/Macromolecules Article

Sustainable In-Water Synthesis of Aliphatic Porous Polyazines: A Versatile Platform for Conjugated Aerogels, PolyHIPEs, or Carbon Foams

Tomaž Kotnik, Gregor Žerjav, Zoran Novak, Albin Pintar, and Sebastijan Kovačič*

Cite This: *Macromolecules* 2023, 56, 5642−5650 Read Online

ACCESS | Metrics & More | Article Recommendations | Supporting Information

ABSTRACT: Access to conjugated porous polymers via synthetically sustainable and straightforward routes is highly desirable, as many polymer systems exhibit high performance but require arduous synthetic protocols that rarely pave the way to commercial reality. In this article, we describe an easily fabricated series of novel highly porous poly(Schiff bases) that feature an aliphatic conjugated backbone obtained with low synthetic complexity from simple reagents such as glyoxal and hydrazine monohydrate in water. The effective synthesis enables the preparation of three different functional scaffolds, i.e., aerogels, polyHIPEs (polymerized HIPEs), and even carbon foams from aliphatic poly(azine) (PAZ) networks. The reported synthetic approach is compared to the literature using "green chemistry metrics", such as the *E*-factor and synthetic complexity (SC) index, and shows dramatic improvements. An *E*-factor of up to 0.27 for aerogels or 80 for polyHIPEs and an SC index of 2.7 are much lower than those for poly(arylene)-based conjugated analogues, indicating good scalability, sustainability, and low cost. PAZ materials feature impressive red/near IR-shifted optical absorption band edges, with an electrochemical band gap of 1.45 eV. Aliphatic PAZ scaffolds are characterized by high flexibility compared to aromatic analogues and do not fail at compressive loads of up to 70%. Finally, carbonization at 500 °C leads to highly porous carbonaceous scaffolds with a high N content of up to 29 wt % (21 mmol of nitrogen per gram carbon material).

INTRODUCTION

Aerogels[1,2] and polyHIPEs (polymerized high internal phase emulsions; PHs)[3,4] are two classes of materials that exhibit porosity at different length scales. Aerogels are characterized by record low density, large specific surface area, and mesoporous structures and can be made from almost any material.[5−7] PHs, on the other hand, enjoy great popularity because both the chemistry of the polymer backbone and macroporous properties, i.e., pore volume, pore size distribution, and degree of three-dimensional (3D) interconnectivity, can be easily tuned and controlled.[8] There are also examples where both materials coexist in a hybrid structure.[4] In terms of rational design, the abundant permanent meso- or macroporosity typical of aerogels or PH can be additionally endowed with delocalized π-conjugated building blocks, a typical feature of conjugated polymers.[9−11] The first synthesis of fully π-conjugated aerogels[12−14] and PHs[15,16] was reported a decade ago, and these first examples were demonstrated for visible light-induced heterogeneous photocatalysis or sorption applications. The possibility to fine-tune the structure of conjugated aerogels and PHs at the molecular level has made them a rapidly growing material platform advantageously used in sustainable processes such as light harvesting, optical sensing, energy storage, and gas separation, to name a few.[17,18]

Their synthetic routes and starting monomers are numerous and involve the formation of C−C cross-couplings in a manner that extends π-conjugation. But despite the many reactions available for their synthesis, they are predominantly built up using aromatic rigid monomers as basic building blocks, such as 1,4-substituted benzenes, resulting in various polyarylene networks. Polyarylene-based aerogels or PHs are thus more widespread than their structurally simpler congener, aliphatic conjugated polyenes, e.g., poly(acetylene), or nitrogen-containing analogues, e.g., poly(azine).[19−21] Although a remarkable array of new aerogels or PHs has been developed, one important point remains a challenge: the development of (more) sustainable synthetic methods for their production. Currently, the question of sustainability arises for both types of organic reactions that have been or could be used for synthesis, i.e., metal-catalyzed (e.g., Suzuki, Sonogashira, or Yamamoto) or metal-free reactions (e.g., nitrile cyclization or phenazine ring fusion). In the former, there is a problem of using noble metallic catalysts (e.g., Pd, Rh, or Ni), while the latter are carried out under harsh conditions such as in high-boiling solvents, e.g., *N*,*N*-dimethylacetamide (DMAc), toluene, or

Received: March 9, 2023
Revised: June 22, 2023
Published: July 7, 2023

https://doi.org/10.1021/acs.macromol.3c00437
Macromolecules 2023, 56, 5642−5650

dimethylformamide (DMF), sometimes even in the presence of molten salts ($ZnCl_2$), at temperatures above 300 °C.[9,17,22] All of these reactions produce stoichiometric quantities of hazardous byproducts containing heavy metals and solvent wastes that are difficult to recycle and pose a serious and irreversible toxicity hazard.[23,24] Therefore, the in-water synthesis of conjugated aerogels or PHs without the use of metallic catalysts or organic solvents would significantly improve sustainability and also reduce costs. In this context, the use of substituted benzene-based monomers, which are commonly used to prepare conjugated polymer matrices, presents a particular challenge due to their limited solubility in water.

Herein, we explored another route to conjugated networks and prepared aliphatic poly(azine)-based aerogels and PHs, i.e., nitrogen-containing poly(acetylene) analogues, utilizing metal-free Schiff-base reaction between aliphatic aldehydes and hydrazine. Schiff-base reactions of aromatic aldehydes and amines are well known for the synthesis of conjugated networks using monomers of different compositions, e.g., A2 + B2, A3 + B3, or A3 + B4, but are carried out in organic solvents due to the aromatic core of the monomers. Moreover, when poly(Schiff base) networks are prepared from specialized aromatic monomers containing a "core" with C3 symmetry or more, custom syntheses are required, further driving up costs and affecting sustainability.[25−30] To keep pace with sustainability and reduce the synthetic complexity of monomers for the preparation of a conjugated network, we used a simple A2 + B2 monomer composition, specifically aliphatic glyoxal and hydrazine monohydrate, and performed a Schiff-base reaction in water. While the A2 + B2 monomer composition in polymer synthesis usually leads to the formation of linear, nonporous structures, the use of removable liquid templates,[31,32] such as sol−gel or HIPE templating, around which a poly(Schiff base) network forms by polycondensation, could be a way to create aerogels or PHs based on aliphatic poly(azine) structures.

This manuscript, therefore, addresses the impact of synthetic simplification on the sustainability of the final formation of poly(Schiff base) networks when aliphatic monomers of the A2 + B2 composition are used. We have shown for the first time that it is possible to prepare three different types of poly(azine)-based conjugated scaffolds, i.e., aerogels, polyHIPEs, or even carbonized analogues by a simple Schiff-base reaction between hydrazine monohydrate (**1**) and glyoxal (**2**) in water (see Figure 1). The sustainability of this in-water synthesis by defining the environmental factor (E) and the synthetic complexity index (SC) as well as the relationship between synthesis structure and properties for each functional material are also discussed.

■ EXPERIMENTAL SECTION

Materials. The monomers were glyoxal (40%; Sigma-Aldrich) and hydrazine (65%; Thermo Fisher Scientific, Alfa Aesar). The surfactant was a commercial triblock copolymer based on poly(ethylene oxide) (PEO) and poly(propylene oxide) (PPO) (Pluronic F-127, a PEO-b-PPO-b-PEO with 70% PEO and a molecular weight of 12,600 g mol^{-1}, Sigma-Aldrich). The solvents used were cyclohexane (≥ 99%; Sigma-Aldrich) and dimethylformamide (≥99%; Sigma-Aldrich). Acids to catalyze dehydration were glacial acetic acid (≥99.8%; Carlo Erba), trifluoroacetic acid (99%; Merck), hydrochloric acid (37%; Merck), and sulfuric acid (95−97%; Sigma-Aldrich).

Synthesis: Polyazine (PAZ)-Based Aerogels, polyHIPEs, and carboHIPEs. The detailed description and corresponding recipes are included in the SI. Briefly, glyoxal and hydrazine monohydrate were added sequentially to the aqueous reaction medium, followed by the addition of a catalytic amount of various acids, and gelation occurred within minutes. Gel points were determined by a simple vial-inversion test, noting the time at which the emulsion stopped flowing. For polyHIPEs, vegetable oil served as the templating agent and was added dropwise to the aqueous solution of glyoxal and hydrazine monohydrate with constant stirring. The prepared O/W HIPEs were polymerized in an oven at 70 °C. The as-prepared dimensionally stable monoliths were then placed in 96% ethanol (v/v) for at least 4 days, and the ethanol was renewed daily. When the ethanol discolored, drying with supercritical CO_2 ($scCO_2$) was performed in both cases. For dehydration, after $scCO_2$ purification/drying, the monoliths were immersed in an aqueous AcOH solution, allowed to stand for 1 day, and then washed several times with water and dried. The monoliths were then also carbonized in an Oxford quartz reactor under an argon atmosphere to produce carbonized polyHIPEs. The resulting materials are referred to as PAZ-X-Y, where X is either the molar concentration of sol in the case of aerogels or the abbreviation for polyHIPEs such as PH. Y refers either to the solvent in which the synthesis occurred, i.e., H_2O or DMF, or to the dehydrated sample labeled as D. The carbonized polyHIPE monoliths were abbreviated as carboHIPEs.

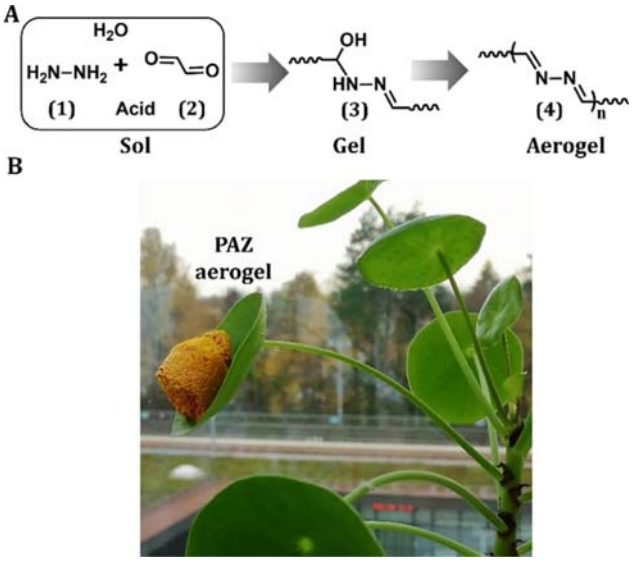

Figure 1. Synthetic route for the preparation of polyazine (PAZ) (A) and the photo of the PAZ aerogel monolith (B).

Characterization. NMR spectroscopy was performed on a Bruker Avance 400 MHz spectrometer. In ^{13}C CP/MAS NMR spectroscopy, the 4 mm CP-MAS probe with $^{1}H-^{19}F$ and $^{31}P-^{15}N$ coils and a maximum spinning rate of 15 kHz with a delay time of 2 s was used. Chemical shifts are given in ppm relative to adamantane as an external standard. NMR data were processed using MestReNova software. FTIR spectroscopy was performed on the dried ground samples using a PerkinElmer (Inc., Waltham, MA) Frontier FTIR spectrometer with attenuated total reflection (ATR) in a 500−3500 cm^{-1} range at a resolution of 4 cm^{-1}. The presented spectra are an average of 32 consecutive measurements on a Ge crystal. Scanning electron microscopy images (SEM) were performed on a JWS-7515, JEOL Ltd. scanning electron microscope. The samples were attached to a carbon tab for better conductivity, and afterward, a thin layer of Pt was sputtered on a sample's surface prior to scanning analysis (for SEM investigations). Nitrogen physisorption analysis was determined from the adsorption and desorption isotherms of N_2 at −196 °C using a TriStar II 3020 instrument (Micromeritics Instrument, Norcross, GA). The specific surface area of the samples was calculated by applying the BET theory to the nitrogen adsorption data within the 0.06−0.30 P/P_0 range. PolyHIPE density (ρ_{PH}) was determined using the gravimetric method by measuring the mass-to-volume ratio of

https://doi.org/10.1021/acs.macromol.3c00437
Macromolecules 2023, 56, 5642−5650

Table 1. Properties of Aerogels and PolyHIPEs[d]

	PAZ-2-H_2O	PAZ-2-DMF	PAZ-PH-H_2O	PAZ-PH-DMF
yield, %[a]	63	47	61	56
ρ_B, g/cm^3[b]	0.12	0.19	0.15	0.06
ρ_P, g/cm^3[c]	1.747	1.8199	1.534	1.433
P, %[e]	93	90	91	96
$d_v \pm \sigma$, μm[f]	5	0.08	28 ± 9	24 ± 8
SSA, m^2/g[g]	37	268	28	200

[a]Yield of polymerization. [b]Dry bulk density. [c]Polymer density determined by a pycnometer. [d]Dry polyHIPE density. [e]Total porosity. [f]Void diameter determined from SEM pictures of broken samples. [g]Specific surface area.

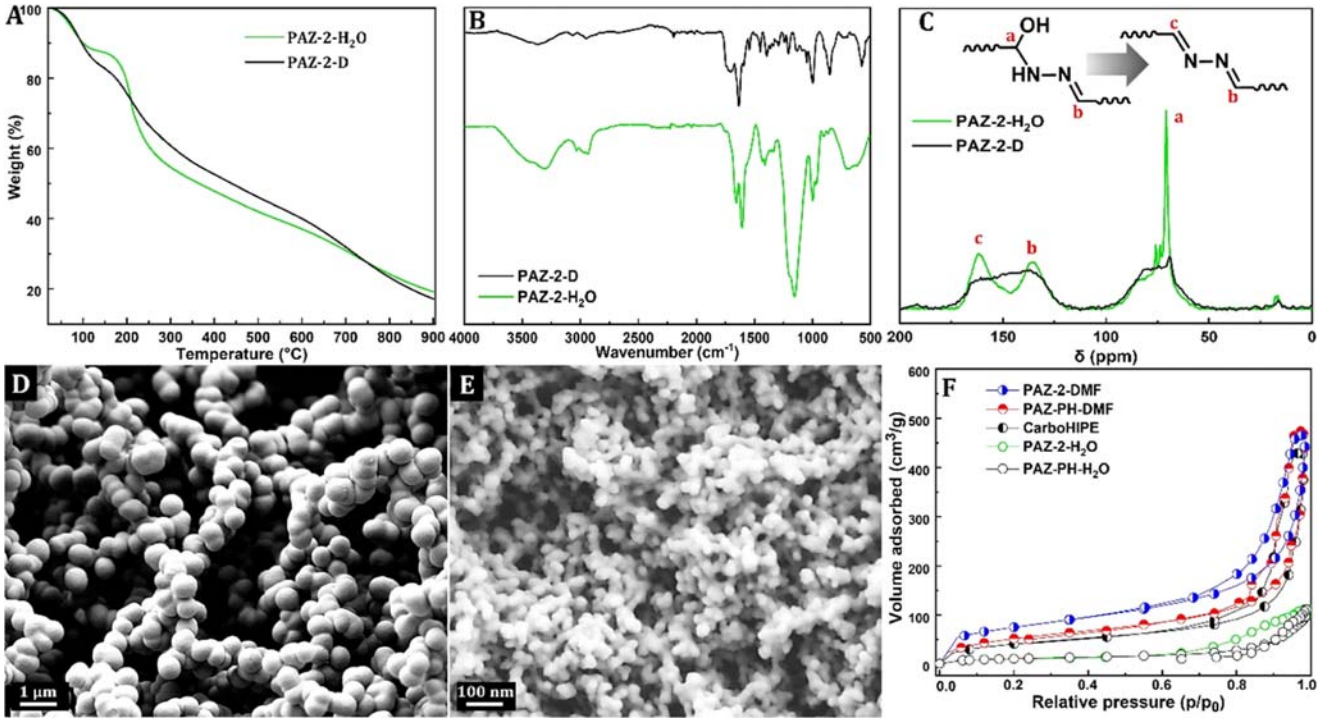

Figure 2. TGA (A), FTIR spectra (B), ^{13}C CP/MAS NMR spectra (C), and SEM images of PAZ-2-H2O (D) and PAZ-2-DMF (E) and N_2 sorption isotherms (F) of PAZ materials.

cubes of approximately 1 cm × 1 cm × 1 cm. The polymer densities (ρ_P; an average of 10 consecutive measurements) were evaluated using a fully automated, highly precision helium pycnometer (Ultrapyc 5000 by Anton Paar). Thermogravimetric analysis (TGA) was carried out using a TGA/DSC 1 STARe System from Mettler Toledo in an airflow and a heating rate of 10 °C/min. Cyclic voltammograms were taken on a Metrohm Autolab PGSTAT302 N (the Netherlands) potentiostat/galvanostat (scan rate: 100 mV/s, T: 25 °C) in a three-electrode electrochemical cell. UV−vis DR spectroscopy analysis was performed on a PerkinElmer Lambda 35 UV−vis spectrophotometer equipped with an RSA-PE-19 M Praying Mantis accessory for powdered samples in order to record the UV−vis diffuse reflectance spectra of the prepared materials. The background correction was performed with a white reflectance standard Spectralon© (range of 200−900 nm).

Solvent Stability Test. To determine solvent resistance, the solubility of PAZ-2-H_2O and PAZ-2-D was tested in different solvents such as H_2O, MeOH, EtOH, THF, or DMF. 10 mg of each sample (PAZ-2-H_2O or PAZ-2-D) was suspended in 1 mL of solvent and heated overnight at 60 °C. The solutions of the two samples were filtered and analyzed by ^{1}H NMR.

RESULTS AND DISCUSSION

Aerogel Synthesis. As shown in Figure 1A, aliphatic and azine-linked π-conjugated aerogels (PAZs) (**4**) were prepared by a simple synthetic protocol using a sol consisting of hydrazine monohydrate (**1**), glyoxal (**2**), and a catalytic amount of acid. Variations in sol concentration (2, 3, or 4 mol·L^{-1} samples, abbreviated as PAZ-2, PAZ-3, and PAZ-4, respectively) and acid strength (HCl ($pK_a \approx -5.9$), H_2SO_4 ($pK_a \approx -2.8$), TFA ($pK_a \approx 0.5$), and AcOH ($pK_a \approx 4.7$)) were studied to monitor their influence on polymerization yield and gelation time (Table S1). The reaction (gelation) between (**1**) and (**2**) occurred immediately when (**1**) was added to the aqueous solution of (**2**), regardless of the sol concentration, and the initially translucent sol became opaque and yellowish. PAZ-2 showed a polymerization yield of about 64% (according to eq S1), which increased with increasing sol concentration to 70 and 76% for PAZ-3 and PAZ-4, respectively (Table S2). On the other hand, the gelation rate and the color of the final gel were found to be directly related to the acid strength. The gel points were reached between 1 and 4 min (Table S1), and the aerogels became yellow-to-light brown for organic acids (AcOH and TFA) and more intense brown for mineral acids

https://doi.org/10.1021/acs.macromol.3c00437
Macromolecules 2023, 56, 5642−5650

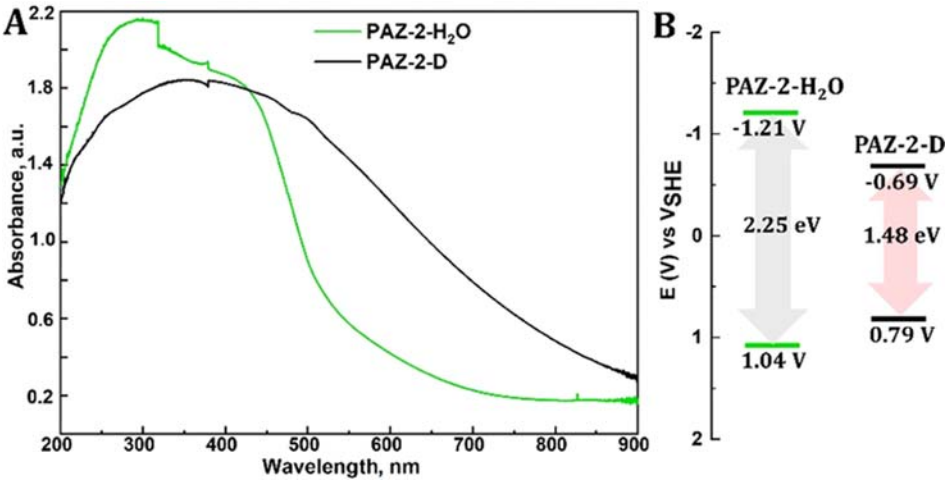

Figure 3. UV−vis DRS spectra (A) and energy band diagrams (B) of the PAZ-2 aerogel.

(HCl and H_2SO_4; Figure S1). Final curing at 70 °C for a further 5 h and subsequent purification/drying using supercritical CO_2 ($scCO_2$) resulted in lightweight and monolithic PAZ aerogels (Figure 1B). The color changes in the reaction of (**1**) and (**2**) indicate a two-step sequence in the synthesis mechanism, with the first step leading to a carbinolamine addition product (**3**) (white to yellowish coloration), while the second, acid-catalyzed dehydration (condensation) step forms a conjugated macromolecular PAZ structure (**4**) (yellow-to-brownish coloration). The latter suggests that the stronger the acid, the more successful the dehydration of (**3**) and thus the extension of the π-conjugation, which was also confirmed by ssNMR (see below). The sol concentration of 2 mol·L^{-1} using AcOH as a catalyst proved to be the most promising formulation in terms of fast gelation and good yield, so the PAZ-2-H_2O aerogel was used for further detailed characterization. PAZ-2-H_2O exhibited a low dry bulk density (ρ_B) of ∼0.12 g·cm^{-3}, indicating that limited volume shrinkage from alcogel to aerogel occurred during the $scCO_2$ process. A high overall porosity of > 90% was calculated from the ρ_B and skeletal density (ρ_P) of ∼1.8 g·cm^{-3}. For comparison, we used DMF as a solvent for the synthesis of the aerogels and determined the polymerization yields, ρ_B, and ρ_P (Table 1) and further compared the sustainability of these syntheses in DMF with those in water (vide infra). Gelation of the DMF-based sol in the presence of AcOH as a catalyst occurred immediately, and the gel point was reached at about the same time as in water. The final curing at 70 °C for another 5 h resulted in monolithic PAZ-2-DMF aerogels, which, however, exhibited a more intense, i.e., dark brown, color compared to the yellow-colored monoliths obtained in water (Figure S2). We believe that the color change is due to more efficient condensation of the macromolecular network in DMF than that in water, converting the carbinolamine structural units (**3**) into an extended π-conjugated electron system with integrated azine units (**4**). Moreover, the efficient condensation in DMF also affects the polymerization yield value, which is lower in PAZ-2-DMF than that in PAZ-2-H_2O (Table 1), probably at the expense of greater water loss.

In another experiment, the PAZ-2-H_2O monolith was immersed in the aqueous AcOH solution after $scCO_2$ purification/drying and left for post-polymerization condensation. The yellow to brown coloration indicated successful condensation of the monolith, which was further abbreviated as PAZ-2-D. The extent of post-polymerization condensation was analyzed by determining the mass losses (water extraction at about 100 °C) before and after acid hydrolysis using thermogravimetric analysis (TGA). The TGA of PAZ-2-H_2O showed a mass loss of about 13 wt %, while the weight loss of PAZ-2-D was negligible at this temperature, indicating the successful elimination of the carbinolamines from the macromolecular network (Figure 2A).

Molecular and Porous Structure. The chemical identity of the PAZ-2-H_2O and PAZ-2-D aerogels was confirmed by a combination of IR spectroscopy, ^{13}C and ^{15}N CP/MAS NMR spectroscopy, and elemental analysis (EA), providing a complete picture of the structure. FTIR spectra displayed several characteristic features of PAZ-2-H_2O. The characteristic stretching band for the N−N functionality is visible at 1010 cm^{-1}, while the absorption band, localized at 1610 cm^{-1}, is characteristic of the azomethine −CH═N− linkage. The absorption band at 1653 cm^{-1} is due to imines near chain ends or not in conjugation within the macromolecular system. An intense peak at 1165 cm^{-1} is attributed to C−O stretching accompanied by a broad absorption at 3200 cm^{-1} attributed to OH vibration at hydration sites within the carbinolamine structural unit that is almost absent in the PAZ-2-D sample (Figure 2B). The PAZ macromolecular networks were further investigated by solid-state NMR. The ^{13}C CP/MAS NMR spectrum of both PAZ samples showed characteristic signals of the azine carbons at 163 and 136 ppm, with the lower field peak assigned to the highly conjugated carbon, while the higher field peak is assigned to the azine carbon at the ends of the conjugated segments or not in conjugation with the system. The PAZ-2-H_2O sample also shows carbon atoms in the carbinolamine structural unit (NH−$\underline{C}H_2$−OH) with a peak at 73 ppm (Figure 2C), while the same peak is significantly reduced in the PAZ-2-D sample. No peak is seen in the 180−200 ppm range that can be assigned to the remaining aldehyde end groups, which is probably due to the fact that the glyoxal used is supplied as a 40% aqueous solution and is not present as a dialdehyde but rather as a mixture of different hydrates.[33,34] Subsequently, ^{15}N CP/MAS NMR was determined, and PAZ-2-H_2O has a peak at 354 ppm, which was assigned to imine nitrogen, and a peak at 140 ppm, which is assigned to the amine nitrogen of carbinolamine (Figure S3).

https://doi.org/10.1021/acs.macromol.3c00437
Macromolecules 2023, 56, 5642−5650

The elemental composition reveals an exceptionally high nitrogen content, as shown by the data for EA of PAZ-2-H_2O which is C 36.8%, H 5.7%, N 42.6%, and O 14.5% (Table S3), corresponding to 30.6 mmol of nitrogen per gram of the material, resulting in an empiric sum formula of $CH_2NO_{0.33}$, i.e., approximately every other atom in the polymer backbone is nitrogen.

Figure 2D,E shows the SEM images of the morphologies of PAZ-2-H_2O and PAZ-2-DMF. Both exhibit a highly porous structure but at different length scales. PAZ-2-H_2O is predominantly macroporous, while PAZ-2-DMF has a mesoporous structure with pores of about 5 μm and 30 nm in diameter, respectively. The porous structure can also be seen in the shape of the isotherms in Figure 2F. PAZ-2-H2O exhibits a steep increase in N_2 sorption uptake at $P/P_0 \approx 0.8$, indicating the presence of macropores, and the presence of a hysteresis loop also indicates the presence of some mesoporosity and thus a somewhat higher specific surface area, i.e., an S_{BET} of 37 $m^2 \cdot g^{-1}$, than that expected for typically macroporous materials. The N_2 sorption isotherm of PAZ-2-DMF showed adsorption/desorption behavior typical of mesoporous materials, with more or less pronounced hysteresis loops and an S_{BET} of 268 $m^2 \cdot g^{-1}$ (Figure 2F).

Optoelectronic Properties. The optoelectronic properties of the PAZ materials were further investigated by UV−vis DRS and cyclic voltammetry (CV), determining the optical absorption band edges, the positions of the frontier orbitals (HOMO/LUMO), and the corresponding band gap energies (Figure 3). The UV−vis DRS spectra of PAZ-2-H_2O show an absorption band edge at 566 nm and that of PAZ-2-D at 880 nm (Figure 3A). The profiles of the frontier orbitals (HOMO/LUMO) positions are further shown in Figure 3B for both samples and were calculated from the difference between the E_{ox} and E_{red} values obtained by the CV analysis (Figure S4). The CV profiles revealed the position of the HOMO at +1.04 and +0.79 V, while the LUMO level was at −1.21 and −0.69 V, corresponding to the electrochemical band gaps of about 2.25 and 1.48 eV for PAZ-2-H_20 and PAZ-2-D, respectively (Figure 3B). It is evident that we have succeeded in extending the conjugation of the macromolecular network by post-polymerization condensation, as the edge of the optical absorption band in PAZ-2-D has been bathochromatically shifted by about 320 nm from 566 to 880 nm, which further narrows the electrochemical band gap by about 0.77 eV from 2.25 to 1.48 eV.

Environmental (E) Factor and Synthetic Complexity (SC). Having established the synthesis protocol, in which the Schiff-base reaction proceeds in water and purification via $scCO_2$, we were interested in evaluating its sustainability. Therefore, among many known green metrics, we decided on the most popular Sheldon's environmental impact factor, known as *E*-factor,[35] and the less known level of synthetic complexity (SC)[36] to be determined. For comparison, DMF as a solvent for synthesis was also evaluated for sustainability. First, the *E*-factor was calculated by measuring the total amount of chemical waste produced relative to the kilogram of the product.[37,38] The PAZ aerogels synthesized in water and purified by $scCO_2$ had an *E*-factor between 0.11 and 0.27 (varies according to sol concentration, see Table S11), whereas the *E*-factor for the aerogels synthesized in DMF was up to 25. As shown in Table S17, we also compared other synthetic routes for the preparation of azine-linked conjugated polymers from the literature. Based on the *E*-factors, which have values as high as 3578, they are far from sustainable given an ideal *E*-factor of 0. Therefore, it is obvious that our synthesis protocol, either water- or DMF-based, is much more sustainable than the state of the art because it is less mass-intensive and generates less organic waste and the *E*-factor is several orders of magnitude lower (see the SI).[39]

Since our PAZ-based aerogels are derived from simple raw materials and the synthetic route is straightforward and cost-effective, they are attractive for large-scale production. To evaluate the potential scalability and commercialization of our PAZ aerogels, we thus calculated the SC index developed by Po et al. (eq S2 and S3).[36,40] This index serves as a rough guide that takes into account several factors affecting the final cost, such as (i) the number of synthesis steps (NSS), (ii) the total yield (RY), (iii) the number of hazardous chemicals used (NHS), (iv) the number of purifications (NUO), and (v) the number of column chromatographic purifications required (NCC) and weights them according to their contribution. The SC index of the PAZ aerogel synthesized in water was calculated and found to be lower than 2.70 on a scale of 1−100 (see the ESI). In the case of DMF, the SC index increased only slightly to 2.96, which is still significantly lower than the literature. Since the *E*-factor and SC index of the PAZ-2 aerogel obtained in DMF were much lower (*E*-factor as low as 25 and an SC of 2.96) than the literature, the porous structure was further characterized. Clearly, our synthesis approach using simple (A2 + B2 composition) and low-cost raw materials, i.e., glyoxal and hydrazine monohydrate, is not only environmentally friendly but also very simple, as the SC index, despite DMF, is significantly lower than similar synthetic routes described in the literature for other conjugated polymers. As such, it offers great potential for industrial scalability.[36]

Solubility Test. Since these PAZ aerogels are synthesized by the A2 + B2 monomer composition and thus consist of linear chains that have no cross-linking points, their solvent resistance is important. Therefore, the solubility of PAZ-2-H_2O and PAZ-2-D was tested in different solvents such as H_2O, MeOH, EtOH, THF, or DMF, and the solutions were analyzed by ^{1}H NMR. The PAZ-2-D sample solution turned yellowish in DMF (Figure S7), but otherwise, no color change was observed in any of the cases. The ^{1}H NMR spectra of the PAZ-2-H_2O sample solutions showed no signal other than D_2O at 4.65 ppm (Figure S7), and the same applies to PAZ-2-D except for the yellowish DMF solution. In the latter case, we observed some additional peaks, probably due to short oligomers (Figure S7), but their amount is negligible, as they were hardly detectable by ^{1}H NMR. The reason for the insolubility is probably the carbinolamine structural units in the PAZ-2-H_2O networks, which allow interaction between the linear chains by H-bonding. However, in PAZ-2-D, this structural unit is largely, though not completely, eliminated through post-polymerization condensation, with some short-chain oligomers now becoming partially soluble, as seen in the DMF experiment, but the macromolecular network as a whole remaining insoluble. The latter is no longer attributed to H-bonding, but the predominant effect is likely to be $\pi-\pi$ stacking between polymer chains within the PAZ macromolecular network due to electronic interactions that are a result of the extended conjugation in the PAZ-2-D sample.

PolyHIPE Synthesis. To demonstrate the versatility of the synthetic approach, we continued our investigations into the preparation of macroporous aliphatic azine-linked PHs through

https://doi.org/10.1021/acs.macromol.3c00437
Macromolecules 2023, 56, 5642−5650

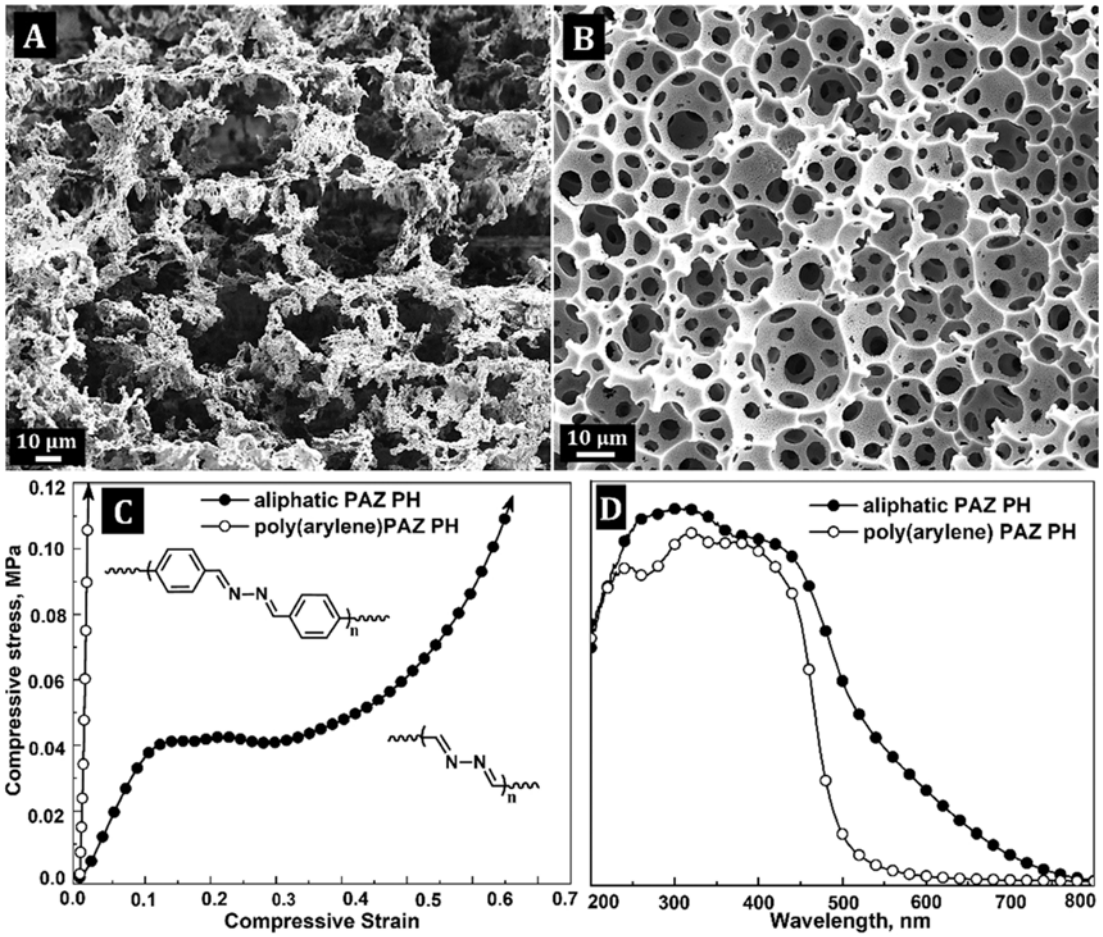

Figure 4. SEM images of PAZ-PH-H_2O (A) and PAZ-PH-DMF (B). Mechanical behavior (C) and UV−vis DRS spectra (D) of PAZ-PH-DMF.

emulsion templating. Oil-in-water (O/W) HIPEs were used as structural templates, although this emulsion system is the least sustainable and green due to the large volume of the oil (droplet) phase. However, since we wanted to be as environmentally friendly as possible, we prepared a HIPE in which a vegetable oil was emulsified into the aqueous acetic acid solution containing (**1**) and (**2**), and this biphasic system was stabilized by Pluronic F−127 as a surfactant (referred to as PAZ-PH-H_2O). Schiff-base condensation in the aqueous acetic acid solution occurred immediately when (**1**) was added to the HIPE with the gel point being reached in a few minutes. Since the reaction between (**1**) and (**2**) is very fast, which often results in phase separation, we first prepared a stable HIPE, i.e., the inner phase was added to the external phase consisting of solvent, glyoxal, and surfactant, and hydrazine was added at the end. Final curing at 70 °C was followed by purification/drying using $scCO_2$, resulting in brown PAZ-PH-H_2O monoliths (Figure 5A). The calculation of the *E*-factor resulted in a value of 79, which is significantly higher than that of the synthesis process for the production of PAZ-2-H_2O aerogels (*E*-factor between 0.11 and 0.27). The polymerization yield (eq S1) was over 60%, the PH density (ρ_{PH}) was 0.15 g·cm^{-3}, the porosity was 91%, and the S_{BET} of about 28 m^2·g^{-1}. The porous structure can be seen in the SEM image in Figure 4A. There are voids about 30 μm in diameter, but it is not a typical 3D-interconnected PH structure, consisting of quasi-spherical voids connected by numerous much smaller circular "holes" called windows.[41] Therefore, we further investigated the emulsion system by replacing the vegetable oil-based O/W HIPEs with the oil-in-oil (O/O) system, namely, cyclohexane-in-DMF HIPE (referred to as PAZ-PH-DMF), which was established in our recent studies.[42,43] A great improvement in the PH structure was achieved, showing a typical 3D-interconnected morphology with average void and window sizes of 24 ± 7 and 3 ± 1 μm, respectively (Figure 4B). The ρ_{PH} was lower at about 0.06 g·cm−^{3}, which reflected in a higher porosity of 96% and a significantly higher S_{BET} of about 200 m^2·g^{-1} (Figure 2F). Although the HIPE system was oil-only, the sustainability did not deteriorate drastically, as the *E*-factor even decreased from 79 to 65, but it is still much higher than that in the water-based aerogel synthesis.

Not only the synthesis and porosity but also the mechanical and optoelectronic properties of these aliphatic PAZ-PHs are interesting in comparison to the poly(arylene) congeners we have recently published.[21] Compressive stress−strain tests on PAZ-PH-DMF monoliths revealed mechanical behavior typical of PH foams with a linear elastic region at low strains (~10%) and a stress plateau region between 15 and 40% strain, where the structure starts to collapse in an accordion-like manner. The robustness of these aliphatic PAZ-PH-DMF samples has been proven by the fact that they can reach strains of up to 70% without failing (Figures 4C and S5). For comparison, poly(arylene)-based PAZ-PHs, whose macromolecular structure consists of aryl building blocks from our previous study,[43] were also subjected to compressive stress−strain tests (Figures 4C and S5). These monoliths were stiffer and brittle, breaking

https://doi.org/10.1021/acs.macromol.3c00437
Macromolecules 2023, 56, 5642−5650

into pieces already at 20% strain (Figure S5). On the other hand, the compressive modulus of aliphatic PAZ-PH-DMF samples (0.32 MPa) is similar to those obtained for elastomeric PH foams[44] and is more than an order of magnitude smaller than that of poly(arylene)-based PAZ-PHs (10 MPa). These results reflect the aliphatic contribution to increasing the flexibility of the π-conjugated macromolecular network of PAZ-PH-DMF monoliths resulting from the choice of a simple aliphatic A2 + B2 monomer combination as building blocks, rather than the aromatic precursors commonly used in the literature. Also of interest are the UV−vis DRS and CV results, which show that elimination of the aromatic building block from the macromolecular network results in a bathochromatically shifted optical absorption band edge by about 105 nm from 505 to 610 nm (Figure 4D) and narrows the electrochemical band gap by about 1.25 eV from 2.73 to 1.48 eV, compared to poly(arylene)-based PAZ-PHs.[21] As with the PAZ aerogels, the solubility test was also performed for the aliphatic azine-linked PHs. When a piece of the PAZ-PH-DMF sample was suspended in DMF and stirred at 60 °C overnight, both the shape and PH morphology of the sample remained unchanged, as confirmed by ^{1}H NMR and SEM microscopy (Figure S8).

Carbon Foam Preparation. Finally, we briefly explored the extent to which the monoliths PAZ-PH-DMF and PAZ-2-DMF can serve as precursors for the preparation of carbon foams referred to as carboHIPEs or carbon-aerogel. Both were successfully prepared at 500 °C. The monoliths did not change their morphology after carbonization and retained the 3D-interconnected macroporous or mesoporous structure typical of PH and aerogel, respectively (Figure 5B,C), although the mass and volume of the sample were significantly reduced (Figure 5A). The SEM micrograph revealed windows-on-void feature characteristic of the PHs, which were preserved in the carboHIPE sample with average void and window sizes of 5 ± 1 and 2 ± 0.8 μm, respectively (Figure 5B) and a pore diameter of 30 nm for the carbon-aerogel structure. Furthermore, the voids of carboHIPEs retained the highly mesoporous walls, forming a hierarchical macro-mesoporous architecture (Figure S6). The dry bulk densities were 0.17 and 0.30 g·cm^{-3} and S_{BET} was still 170 and 262 m^2·g^{-1} for carboHIPEs and carbon-aerogel, respectively. Moreover, the elemental composition shows that a considerable nitrogen content of about 29 wt % was maintained for both materials, corresponding to 20.7 mmol of nitrogen per gram of the carbon material. The facilely prepared PAZ-derived carbon foams are promising not only because of their advantageous properties such as highly porous PH or aerogel morphology, structural stability, and high N content but also because of the tremendous potential in photoelectrocatalytic applications, which are currently being investigated in our laboratory.

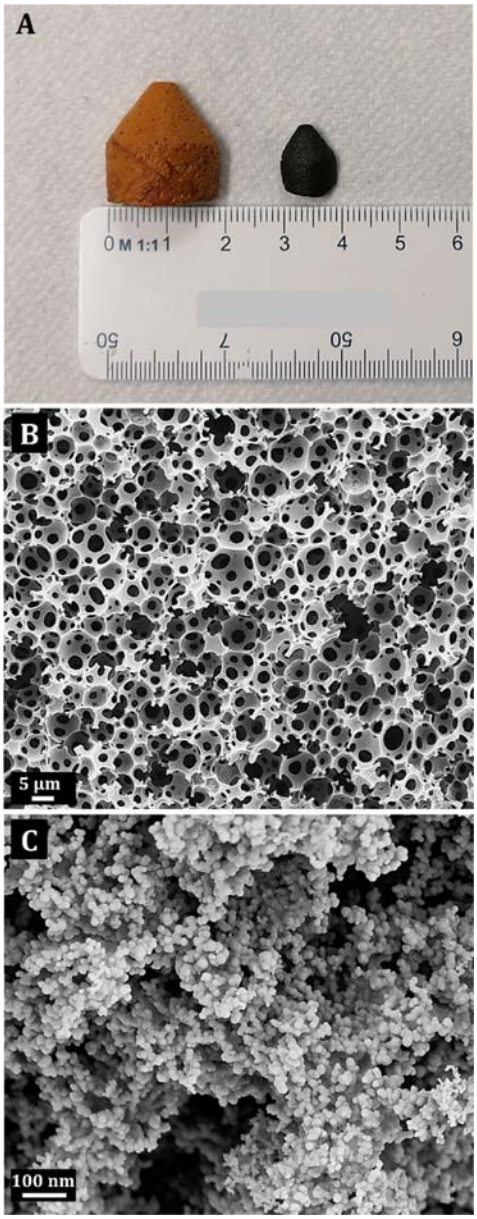

Figure 5. Photo of PH and carbon foam monoliths (A). SEM images of carboHIPE (B) and carbonized aerogel (C).

CONCLUSIONS

In summary, the concept of a simple, low-cost, and green synthesis process has been demonstrated for the fabrication of a series of highly porous PAZ-based materials, namely, aerogels, polyHIPEs, and carbon foams. The synthesis involves low-cost raw materials, e.g., glyoxal and hydrazine monohydrate in water, with a low SC index of 2.7 and low chemical waste production with an *E*-factor of only 0.27 for aerogels or 80 for polyHIPEs. All three functional materials, i.e., aerogels, polyHIPEs, and carbon foams, consist of three-dimensional networks with a highly interconnected meso-macroporous morphology, a high porosity of >90%, and a specific BET surface area of up to 268 m^2·g^{-1}. Mechanical studies for PHs show the influence of the aliphatic content on macromolecular flexibility with mechanical behavior similar to that of flexible foams, reaching strains of 70% without failure. Finally, the carbonization of aerogels or PHs on the other hand allows us to obtain nitrogen-doped carbon foams with an exceptionally high N content of up to 21 mmol of nitrogen per gram of the carbon material.

We are confident that chemistry based on aliphatic A2 and B2 monomers, liquid templates, and supercritical CO_2 drying provides an attractive platform for the synthesis of conjugated porous polymers or carbon foams in a sustainable and cost-effective manner.

https://doi.org/10.1021/acs.macromol.3c00437
Macromolecules 2023, 56, 5642−5650

■ ASSOCIATED CONTENT

Supporting Information

The Supporting Information is available free of charge at https://pubs.acs.org/doi/10.1021/acs.macromol.3c00437.

Description of synthesis procedures and details about characterization (Word) (PDF)

■ AUTHOR INFORMATION

Corresponding Author

Sebastijan Kovačič − *National Institute of Chemistry, SI-1001 Ljubljana, Slovenia;* orcid.org/0000-0003-2664-9791; Email: sebastijan.kovacic@ki.si

Authors

Tomaž Kotnik − *National Institute of Chemistry, SI-1001 Ljubljana, Slovenia*

Gregor Žerjav − *National Institute of Chemistry, SI-1001 Ljubljana, Slovenia*

Zoran Novak − *Faculty of Chemistry and Chemical Engineering, University of Maribor, SI-2000 Maribor, Slovenia;* orcid.org/0000-0001-6677-0743

Albin Pintar − *National Institute of Chemistry, SI-1001 Ljubljana, Slovenia*

Complete contact information is available at: https://pubs.acs.org/10.1021/acs.macromol.3c00437

Notes

The authors declare no competing financial interest.

■ ACKNOWLEDGMENTS

This work was supported by the Ministry of Education, Science and Sport of the Republic of Slovenia and the Slovenian Research Agency (grants P2-0150, P2−0046, and N2-0166).

■ REFERENCES

(1) Kistler, S. S. Coherent Expanded Aerogels and Jellies. *Nature* **1931**, *127*, 741.

(2) Hüsing, N.; Schubert, U. Aerogels - Airy Materials: Chemistry, Structure, and Properties. In *Angewandte Chemie, International Edition*; Wiley-VCH Verlag, 1998; pp 22−45 DOI: 10.1002/(sici)1521-3773(19980202)37:1/2<22::aid-anie22>3.0.co;2-i.

(3) Zhang, T.; Sanguramath, R. A.; Israel, S.; Silverstein, M. S. Emulsion Templating: Porous Polymers and Beyond. *Macromolecules* **2019**, *52*, 5445−5479.

(4) Horvat, G.; Kotnik, T.; Žvab, K.; Knez, Ž.; Novak, Z.; Kovačič, S. Silica Aerogel-Filled Polymer Foams by Emulsion-Templating: One-Pot Synthesis, Hierarchical Architecture and Thermal Conductivity. *Chem. Eng. J.* **2022**, *450*, No. 138251.

(5) Jiang, S.; Agarwal, S.; Greiner, A. Low-Density Open Cellular Sponges as Functional Materials. *Angew. Chem., Int. Ed.* **2017**, *56*, 15520−15538.

(6) Ziegler, C.; Wolf, A.; Liu, W.; Herrmann, A. K.; Gaponik, N.; Eychmüller, A. Modern Inorganic Aerogels. *Angew. Chem., Int. Ed.* **2017**, *56*, 13200−13221.

(7) Antonietti, M.; Fechler, N.; Fellinger, T. P. Carbon Aerogels and Monoliths: Control of Porosity and Nanoarchitecture via Sol-Gel Routes. *Chem. Mater.* **2014**, *26*, 196−210.

(8) Foudazi, R. HIPEs to PolyHIPEs. *React. Funct. Polym.* **2021**, *164*, No. 104917.

(9) Lee, J. S. M.; Cooper, A. I. Advances in Conjugated Microporous Polymers. *Chem. Rev.* **2020**, *120*, 2171−2214.

(10) Byun, J.; Zhang, K. A. I. Designing Conjugated Porous Polymers for Visible Light-Driven Photocatalytic Chemical Transformations. *Mater. Horiz.* **2020**, *7*, 15−31.

(11) Qiu, Z.; Hammer, B. A. G.; Müllen, K. Conjugated Polymers − Problems and Promises. *Prog. Polym. Sci.* **2020**, *100*, No. 101179.

(12) Du, R.; Zhang, N.; Xu, H.; Mao, N.; Duan, W.; Wang, J.; Zhao, Q.; Liu, Z.; Zhang, J.; Du, R.; Zhang, N.; Xu, H.; Mao, N. N.; Duan, W. J.; Wang, J. Y.; Zhao, Q. C.; Liu, Z. F.; Zhang, J. CMP Aerogels: Ultrahigh-Surface-Area Carbon-Based Monolithic Materials with Superb Sorption Performance. *Adv. Mater.* **2014**, *26*, 8053−8058.

(13) Ou, H.; Yang, P.; Lin, L.; Anpo, M.; Xinchen Wang, nd.; Ou, H. H.; Yang, P. J.; Lin, L. H.; Anpo, M.; Wang, X. C. Carbon Nitride Aerogels for the Photoredox Conversion of Water. *Angew. Chem.* **2017**, *129*, 11045−11050.

(14) Mu, P.; Bai, W.; Zhang, Z.; He, J.; Sun, H.; Zhu, Z.; Liang, W.; Li, A. Robust Aerogels Based on Conjugated Microporous Polymer Nanotubes with Exceptional Mechanical Strength for Efficient Solar Steam Generation. *J. Mater. Chem. A* **2018**, *6*, 18183−18190.

(15) Slováková, E.; Ješelnik, M.; Žagar, E.; Zedník, J.; Sedláček, J.; Kovačič, S. Chain-Growth Insertion Polymerization of 1,3-Diethynylbenzene High Internal Phase Emulsions into Reactive π-Conjugated Foams. *Macromolecules* **2014**, *47*, 4864−4869.

(16) Zhang, K.; Vobecka, Z.; Tauer, K.; Antonietti, M.; Vilela, F. π-Conjugated PolyHIPEs as Highly Efficient and Reusable Heterogeneous Photosensitizers. *ChemComm.* **2013**, *49*, 11158−11160.

(17) Zhang, Z.; Jia, J.; Zhi, Y.; Ma, S.; Liu, X. Porous Organic Polymers for Light-Driven Organic Transformations. *Chem. Soc. Rev.* **2022**, *51*, 2444−2490.

(18) Sun, J.; Wu, T.; Wu, H.; Li, W.; Li, L.; Liu, S.; Wang, J.; Malfait, W. J.; Zhao, S. Aerogel-Based Solar-Powered Water Production from Atmosphere and Ocean: A Review. *Mater. Sci. Eng., R* **2023**, *154*, No. 100735.

(19) Saxman, A. M.; Liepins, R.; Aldissi, M. Polyacetylene: Its Synthesis, Doping and Structure. *Prog. Polym. Sci.* **1985**, *11*, 57−89.

(20) Roncali, J. Synthetic Principles for Bandgap Control in Linear π-Conjugated Systems. *Chem. Rev.* **1997**, *97*, 173−205.

(21) Maia, L. F.; de Oliveira, V. E.; Edwards, H. G. M.; de Oliveira, L. F. C. The Diversity of Linear Conjugated Polyenes and Colours in Nature: Raman Spectroscopy as a Diagnostic Tool. *ChemPhysChem.* **2021**, *22*, 231−249.

(22) Taylor, D.; Dalgarno, S. J.; Xu, Z.; Vilela, F. Conjugated Porous Polymers: Incredibly Versatile Materials with Far-Reaching Applications. *Chem. Soc. Rev.* **2020**, *49*, 3981−4042.

(23) Sherwood, J.; Clark, J. H.; Fairlamb, I. J. S.; Slattery, J. M. Solvent Effects in Palladium Catalysed Cross-Coupling Reactions. *Green Chem.* **2019**, *21*, 2164−2213.

(24) Fantoni, T.; Bernardoni, S.; Mattellone, A.; Martelli, G.; Ferrazzano, L.; Cantelmi, P.; Corbisiero, D.; Tolomelli, A.; Cabri, W.; Vacondio, F.; Ferlenghi, F.; Mor, M.; Ricci, A. Palladium Catalyst Recycling for Heck-Cassar-Sonogashira Cross-Coupling Reactions in Green Solvent/Base Blend. *ChemSusChem.* **2021**, *14*, 2591−2600.

(25) Schwab, M. G.; Hamburger, M.; Feng, X.; Shu, J.; Spiess, H. W.; Wang, X.; Antonietti, M.; Müllen, K. Photocatalytic Hydrogen Evolution through Fully Conjugated Poly(Azomethine) Networks. *Chem. Commun.* **2010**, *46*, 8932−8934.

(26) Laybourn, A.; Dawson, R.; Clowes, R.; Iggo, J. A.; Cooper, A. I.; Khimyak, Y. Z.; Adams, D. J. Branching out with Aminals: Microporous Organic Polymers from Difunctional Monomers. *Polym. Chem.* **2012**, *3*, 533−537.

(27) Li, G.; Zhang, B.; Yan, J.; Wang, Z. Micro- and Mesoporous Poly(Schiff-Base)s Constructed from Different Building Blocks and Their Adsorption Behaviors towards Organic Vapors and CO 2 Gas. *J. Mater. Chem. A.* **2014**, *2*, 18881−18888.

(28) Xiao, Z.; Huang, X.; Zhao, K.; Song, Q.; Guo, R.; Zhang, X.; Zhou, S.; Kong, D.; Wagner, M.; Müllen, K.; Zhi, L. Band Structure Engineering of Schiff-Base Microporous Organic Polymers for Enhanced Visible-Light Photocatalytic Performance. *Small* **2019**, *15*, No. 1900244.

(29) Segura, J. L.; Mancheño, M. J.; Zamora, F. Covalent Organic Frameworks Based on Schiff-Base Chemistry: Synthesis, Properties and Potential Applications. *Chem. Soc. Rev.* **2016**, *45*, 5635−5671.
(30) Jin, Y.; Zhu, Y.; Zhang, W. Development of Organic Porous Materials through Schiff-Base Chemistry. *CrystEngComm* **2013**, *15*, 1484−1499.
(31) Wu, D.; Xu, F.; Sun, B.; Fu, R.; He, H.; Matyjaszewski, K. Design and Preparation of Porous Polymers. *Chem. Rev.* **2012**, *112*, 3959−4015.
(32) Silverstein, M. S. The Chemistry of Porous Polymers: The Holey Grail. *Isr. J. Chem.* **2020**, *60*, 140−150.
(33) Loeffler, K. W.; Koehler, C. A.; Paul, N. M.; de Haan, D. O. Oligomer Formation in Evaporating Aqueous Glyoxal and Methyl Glyoxal Solutions. *Environ. Sci. Technol.* **2006**, *40*, 6318−6323.
(34) Chaloner-Gill, B.; Cheer, C. J.; Roberts, J. E.; Euler, W. B. Structure of Glyoxal Dihydrazone and Synthesis, Characterization, and Iodine Doping of Unsubstituted Polyazine. *Macromolecules* **1990**, *23*, 4597−4603.
(35) Sheldon, R. A. The E Factor: Fifteen Years On. *Green Chem.* **2007**, *9*, 1273−1283.
(36) Po, R.; Bianchi, G.; Carbonera, C.; Pellegrino, A. "all That Glisters Is Not Gold": An Analysis of the Synthetic Complexity of Efficient Polymer Donors for Polymer Solar Cells. *Macromolecules* **2015**, *48*, 453−461.
(37) Roschangar, F.; Sheldon, R. A.; Senanayake, C. H. Overcoming Barriers to Green Chemistry in the Pharmaceutical Industry − the Green Aspiration Level Concept. *Green Chem.* **2015**, *17*, 752−768.
(38) Sheldon, R. A. Metrics of Green Chemistry and Sustainability: Past, Present, and Future. *ACS Sustainable Chem. Eng.* **2018**, *6*, 32−48.
(39) Sheldon, R. A.; Greenchem; Sheldon, R. A. The E Factor 25 Years on: The Rise of Green Chemistry and Sustainability. *Green Chem.* **2017**, *19*, 18−43.
(40) Penconi, M.; Bianchi, G.; Nitti, A.; Savoini, A.; Carbonera, C.; Pasini, D.; Po, R.; Luzzati, S. A Donor Polymer with a Good Compromise between Efficiency and Sustainability for Organic Solar Cells. *Adv. Energy Sustainability Res.* **2021**, *2*, No. 2100069.
(41) Cameron, N. R.; Sherrington, D. C. High Internal Phase Emulsions (HIPEs) - Structure, Properties and Use in Polymer Preparation. *Adv. Polym. Sci.* **1996**, *126*, 163−214.
(42) Kotnik, T.; Žerjav, G.; Pintar, A.; Žagar, E.; Kovačič, S. Highly Porous Poly(Arylene Cyano-Vinylene) Beads Derived through the Knoevenagel Condensation of the Oil-in-Oil-in-Oil Double Emulsion Templates. *ACS Macro Lett.* **2021**, *10*, 1248−1253.
(43) Kotnik, T.; Žerjav, G.; Pintar, A.; Žagar, E.; Kovačič, S. Azine- and Imine-Linked Conjugated PolyHIPEs through Schiff-Base Condensation Reaction. *Polym. Chem.* **2022**, *13*, 474−478.
(44) Berezovska, I.; Sanguramath, R. A.; Silverstein, M. S. β-Cyclodextrin-Based Macroporous Monoliths: One-Pot Oil-in-Oil Emulsion Templating and Adsorption. *J. Polym. Sci.* **2022**, *60*, 81−89.

https://doi.org/10.1021/acs.macromol.3c00437
Macromolecules 2023, 56, 5642−5650